Zemax Modeling of a Self-aligned Focusing Schlieren System with Simulated Compressible Flow

Nicholas A. Mejia[1,*], Bryan E. Schmidt[1], Brett F. Bathel[2], Joshua M. Weisberger[2], Joel A. McQuaid[3], Christoph Brehm[3], Craig T. Johansen[4]

1: Case Western Reserve University, USA
2: NASA Langley Research Center, USA
3: University of Maryland, USA
4:University of Calgary, CA

*Corresponding author: nicholas.mejia@case.edu

Keywords: ANSYS Zemax, Compressible Flow, Schlieren, Computational Fluid Dynamics, Flow Visualization.

ABSTRACT

A self-aligned focusing schlieren system is simulated in the ANSYS Zemax OpticStudio software environment. The model uses a custom scatter-defining dynamic link library on the retroreflective background in order to scatter rays in the direction of the incident ray rather than the specular ray. Simulated compressible flow refractive index fields are imported into Zemax by use of the grid gradient object and a workaround to the maximum point limit is introduced. The Ronchi ruling is built as a high resolution bitmap image in MATLAB and set in Zemax as a slide object allowing the bitmap image to either transmit or terminate rays at each line pair. The Zemax simulations are compared to computational numerical schlieren and experimental conventional, path-integrated schlieren results from a hypersonic stagnation point injection flow configuration and an experimental image of a shock wave from a laser-induced breakdown. In the stagnation point injection simulations, the Zemax schlieren images capture complex flow features such as the Mach disk, shear layers, contact surface, and bow shock well, but contains long, curved features (striations) between the model and the bow shock that are not present in the synthetic schlieren image from the CFD or the experimental image. The image from Zemax of the spark-induced shock wave captures the shape and curvature of the shock but appears blurry due to grid discretization in the computational data.

1. Introduction

Schlieren imaging is a commonly used flow visualization tool that provides qualitative information about the refractive index gradient in a transparent medium, which is directly related to the density gradient in gases via the Gladstone-Dale relation (Gladstone & Dale, 1863). This makes it particularly applicable for compressible or variable-density flows. Settles (2001) and Settles & Hargather (2017) provide a history of the development of conventional schlieren imaging and a

review of more recent developments. Conventional schlieren uses a focusing mirror or lens to collimate light from a source. The column of light then passes through a measurement volume where gradients of density are present. A mirror or lens on the opposite side of the measurement volume then forms an image of the source where a spatial filter (typically a knife edge) is partially inserted into the image. The portion of light not blocked by the knife edge is then imaged by a camera. The locations of density gradients in the direction orthogonal to the knife edge within the measurement volume appear as either light or dark regions in the schlieren image. This is a result of rays in the collimated light that are refracted as they pass through the measurement volume and then pass over the knife edge or terminate on it, respectively. Adjusting the degree of insertion of the knife edge into the optical path provides adjustment of sensitivity to these gradients. The image acquired by a conventional schlieren system is path-integrated by nature and therefore can include non-pertinent flow features at the extremities of the optical path between the focusing elements. Additionally, the field of view of a conventional schlieren system is limited to the size of the mirrors or lenses being used, and by the optical access available to visualize the measurement volume. Weisberger & Bathel (2022b) discuss these drawbacks and more in detail.

Focusing schlieren is a variant of the conventional schlieren imaging technique that filters out non-pertinent features along the line of sight by imaging a plane with a narrow depth of field. The conventional form of this technique, originally developed in the 1940s by Hartmann (1940), Schardin (1942), and Burton (1949), and later modernized by Weinstein (1993), typically uses a back-illuminated source grid consisting of a regular pattern of opaque and transparent lines. The transparent, light-transmitting lines of the source grid act as multiple extended schlieren light sources. On the opposite side of the measurement volume, a lens forms an image of the source grid onto a cutoff grid, which is a photograph negative of the source grid. Adjusting the offset of the cutoff grid in the plane of the imaged source grid and orthogonal to the source lines provides sensitivity adjustment, similar to a knife edge adjustment in a conventional schlieren system. The narrow depth of field arises from schlieren imaging of a common plane with multiple sources, as well as the focusing properties of the lens, as noted by Boedeker (1959).

A limitation of focusing schlieren systems is the need to precisely align the source and cutoff grids, which can be tedious. Further, any misalignment of the system, whether by user adjustment or environmental vibration, results in loss of sensitivity. Recently, a self-aligned focusing schlieren (SAFS) system was developed that eliminates the need for this alignment procedure to be performed and makes it insensitive to vibration (Bathel & Weisberger, 2021). While a limited number of works have characterized aspects of this SAFS system, some of the general working principles of the instrument are not well understood (N. Mejia & Schmidt, 2023; Hill et al., 2023).

In this work, a SAFS system similar to that developed by Bathel & Weisberger (2021) is modelled in the ANSYS Zemax OpticStudio Professional software environment in order to gain a better understanding of its working principles. In an effort to begin validating the SAFS instrument

model, complex refractive index fields from computational fluid dynamics (CFD) solutions are simulated within the Zemax software, and when available, compared against experimental data. To the authors' knowledge, this is one of the first attempts to import complex refractive index field data into Zemax for the purposes of simulating a non-intrusive optical diagnostic.

2. Simulated Experimental Setup

A schematic of a SAFS system of the kind developed by Bathel & Weisberger (2021) and Weisberger & Bathel (2022b) is shown in Fig. 1. Here, light from a light source is loosely collimated and diffused by a condenser/diffuser lens (CD). The light is then made to be linear vertically polarized (LVP) from a light source by a linear polarizer (LP^1). It is then coupled onto the instrument optical axis by a polarizing beamsplitter (PBS) and back-illuminates a Ronchi ruling (RR). A polarizing Rochon prism (RP) allows the light to pass through without refraction. The LVP light is then passed through a quarter-wave plate (QWP) oriented such that it modifies the polarization from LVP to right circularly polarized (RCP). A field lens (FL) then forms an image of the RR onto a retroreflective background (RBG).

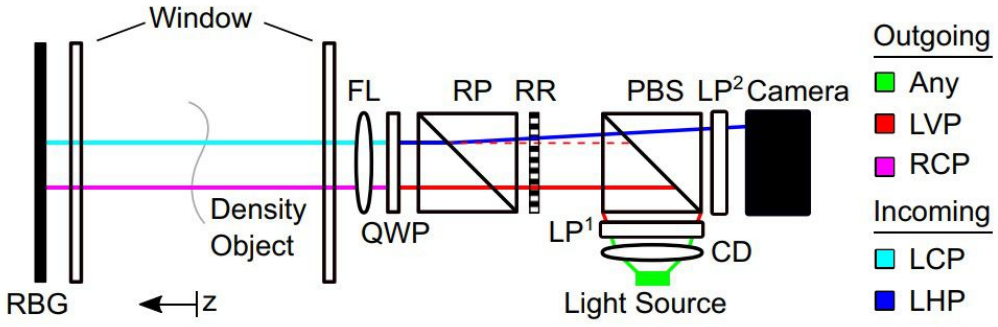

Figure 1. Schematic of the self-aligned focusing schlieren system, adapted from Weisberger & Bathel (2022b).

Upon retroreflection, the handedness of the polarization flips from RCP to left circularly polarized (LCP). The FL then forms an image of the projected RR onto the physical RR. By imaging the projection of the RR back onto itself, the system becomes inherently self-aligned. As the light passes again through the QWP, it is modified from LCP to linear horizontal polarization (LHP) light. Now, as the light passes through the RP, it imparts a small (on the order of arc minutes) angular offset to the returning rays, which provides the offset between the re-imaged projection of the RR (akin to a source grid in a conventional focusing schlieren system) and the physical RR. Since the light is LHP, it can transmit through the PBS and a subsequent linear polarizer (LP^2) that is oriented to pass only LHP light onto an imaging sensor on a camera.

3. Optical Simulation

Zemax is a professional ray-tracing software that is typically used for optical design and offers both sequential or non-sequential modes. The key difference between these two modes is that in non-sequential mode rays do not interact with objects or surfaces in a predefined order, while in sequential mode the sequence of surfaces a ray interacts with is specified. There are other differences, but generally non-sequential mode is considered optimal for analyzing scattering, which must be properly simulated to accurately capture the performance of the retroreflective background in a SAFS system and how it ultimately contributes to the formation of a focused schlieren image. Therefore, the simulations shown in this work use non-sequential mode. The authors are currently unaware of published work where Zemax has been used to test optical system performance with complex refractive index fields and visualize flow fields. However, Settles & Hargather (2017) and Wang & Kulatilaka (2017) both used Zemax to simulate very basic flow-like disturbances to determine how they influence beam steering. The stock Zemax program does not come with premade objects required for a SAFS system, namely the PBS, RP, RR, QWP, RBG, and the DO. The implementation of each of these will be discussed in this section. It is worth noting that the PBS, RP, and RR are relatively simple to implement, but the RBG requires a custom scatter-defining dynamic link library (DLL) to properly simulate its performance. The reader is referred to the ANSYS Zemax OpticStudio User Manual (AZOUM) for greater detail on any of these objects. Additionally, the initial position of each SAFS component was determined using the assistive tool for self-aligning schlieren (ATLAS) (N. Mejia & Schmidt, 2023) and the system uses an ambient air medium.

3.1. Camera, Linear Polarizers, and Field Lens

The camera is implemented into Zemax using a detector rectangle with 1210×800 pixels to match the 1 MP resolution of the experimental images, and is sized to match the form factor of the camera's imaging sensor. The linear polarizers are flat, circular lenses with a Jones matrix filter. The light source was modelled using a Zemax radial source and the condenser-diffuser lens was completely omitted as the rays are pre-defined to be collimated. The field lens is a Zemax stock 3-lens system chosen to match most closely with the operating parameters of the lens used in the physical SAFS system.

3.2. Quarter-Wave Plate

The quarter-wave plate was implemented in Zemax by using a quartz surface with thickness determined by the waveplate-retardance formula in Eq. (1) (Jenkins & White, 1976).

$$\delta = \frac{2\pi}{\lambda} d(n_o - n_e) \tag{1}$$

Here, δ is the phase difference, λ is the wavelength of the incident light, n_o and n_e are the ordinary and extraordinary refractive indexes, and d is the thickness of the crystal. For a quarter-wave plate, $\delta = \frac{\pi}{4}$ while n_o and n_e are available freely in many tabulated sources, so d can be computed directly.

3.3. Rochon Prism and Polarizing Beamsplitter

The Rochon prism and polarizing beamsplitter are each constructed by using two adjacent $30^\circ - 60^\circ - 90^\circ$ triangular prisms that are aligned such that they form a single rectangular prism with the hypotenuse faces in contact with each other. The Rochon prisms used in the physical SAFS system are typically glass-quartz prisms where the refractive index of the glass is as close as possible to that of the quartz (Weisberger & Bathel, 2022a). An ideal glass-quartz Rochon prism (i.e., one that behaves the same regardless of the side upon which light is incident) would have matching indices of refraction for the quartz and glass (Ammann & Massey, 1968). In Zemax the Rochon prism is modeled as an ideal glass-quartz prism by setting both materials to quartz, but only enabling birefrigence on one half to deflect the returning LHP rays. The polarizing beamsplitter is similarly constructed, but is glass-glass and has a custom S-P polarizing coating on the inner face. The procedure to make this coating is available in both the AZOUM and ANSYS Zemax support forums.

3.4. Ronchi Ruling

The Ronchi ruling was built using the slide object, which is a plane surface that allows an uploaded bitmap image to act as a filter. Building a 3D model of a RR was initially attempted, but Zemax became unresponsive during loading of the object due to the large number of line pairs in the model, even for a relatively low frequency of 2 lp/mm. The bitmap for the slide object was created with MATLAB to allow for the generation of high resolution grid patterns that could be easily imported into Zemax. An example of such an implementation in a mid-development build of a SAFS system in Zemax is shown in Fig. 2. Here, the bitmap values of 0 and 1 are represented by black and white vertical lines, respectively. Rays (thin blue lines) that interact with the black lines are terminated at the slide surface while rays that interact with the white lines are transmitted through the slide with no energy loss.

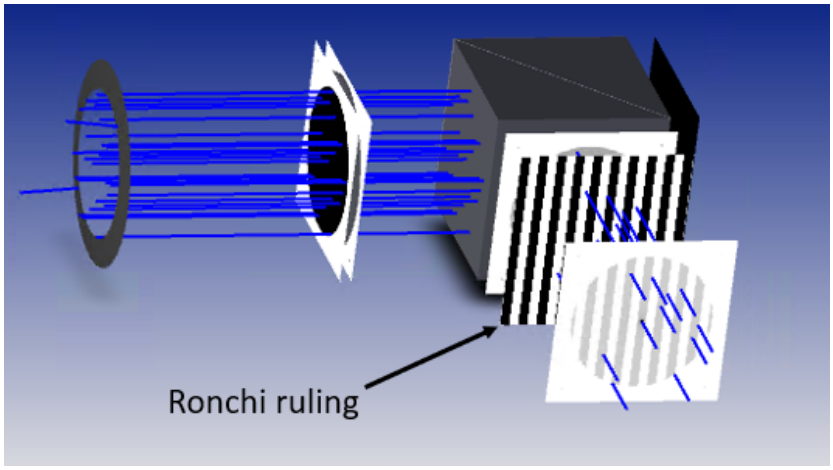

Figure 2. Example of a low frequency Ronchi ruling (labeled) in a mid-development build of a SAFS system in Zemax. Rays (thin blue lines) that interact with bitmap values of 0 (black vertical lines) are terminated, while rays that interact with bitmap values of 1 (white vertical lines) are transmitted with no energy loss.

3.5. Density Object

Implementing a density object with a complex refractive index field requires the use of the grid gradient object (GGO), which is a flat surface with an index of refraction defined for a grid of coordinate points in three dimensions, with the index information stored in an ASCII file with a strict format described in the AZOUM. There is a fairly prohibitive limitation on the number of points in a single GGO which is given by Eq. (2).

$$4 \times 10^9 = 6400 \times n_x \times (1 + n_y + n_y \times n_z) \tag{2}$$

Here, n_x, n_y, and n_z are the number of points on each respective axis within a single GGO. The left hand side (4×10^9) is the 64-bit limit inherent to Zemax, while 1×10^9 is the 32-bit limit. In testing, a single GGO was not sufficient to resolve fine structures in a complex refractive index field, and often CFD solutions and the grids on which they are computed exceed this limit. To bypass this limitation, a method of constructing multiple GGOs adjacent to each other was developed, each of which contains a subdomain of the full field. While there is a limitation on the number of points in a single GGO, there is no limit on the number of GGOs. Increasing the number of GGOs is tedious however, and increases the cost of the simulation significantly. In this work, the density object was constructed from 8 GGOs, each with $n_x = n_y = n_z = 83$ for a total of $4,574,296$ refractive index points in the optical system. Additionally, the 8 GGOs that comprise the density object are surrounded by additional GGOs at an arbitrarily lower point density and set to the ambient refractive index. Without the surrounding ambient GGO, the GGOs containing the refractive index field of interest are observed to refract light rays in a non-physical way.

3.6. Retroreflective background

The retroreflective background is designed using a rectangular surface with a custom user-defined scattering function to mimic the behavior described by Héricz et al. (2017). Zemax provides the user with a few stock scattering models and user-defined models. To simulate an RBG, the stock "Gaussian_XY.dll" function was modified in order to scatter rays with a Gaussian distribution centered about the incident ray path rather than the specular ray path, both of which are illustrated in Fig. 3.

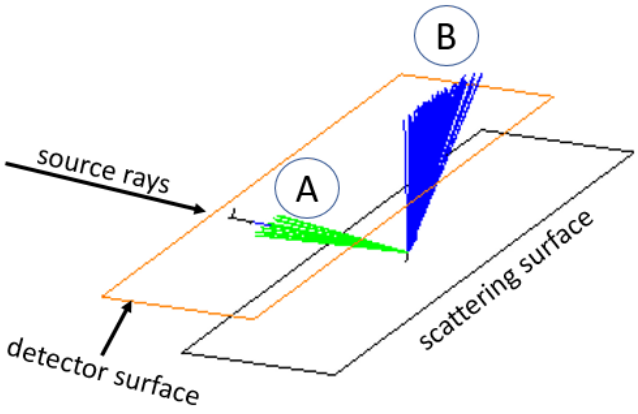

Figure 3. Example of scattering surface in Zemax with modified and original DLL. Scattered rays with direction calculated from the modified DLL (A) return towards the incident (source) rays while those calculated with the original DLL (B) spread about the specular ray path.

Here, two sets of source rays originate along the source ray vector shown. One set of rays interacts with the default "Gaussian_XY.dll" and scatter with a Gaussian distribution along the specular ray path (B), while the correct RBG behavior interacts with the modified 'Gaussian_XY.dll' and is illustrated by the rays that are scattered in the direction of the incident ray path with a Gaussian distribution (A). The width of the Gaussian scattering can then be tuned to match the RBG material properties. Note that rays do not physically interact with the detector surface, and it is just used for the purpose of illustration.

3.7. SAFS Zemax Assembly

A labeled wireframe image of the completed SAFS system as modelled in Zemax is shown in Fig. 4a, and a 3D shaded isometric view is provided in Fig. 4b, where the circular region on the plane of the RBG indicates the area over which an RR is projected. Only a small number of layout rays are used for viewing clarity of the full system. As mentioned earlier, the density object comprises multiple cubes in the system, but each represents a 3D grid of refractive indices specified

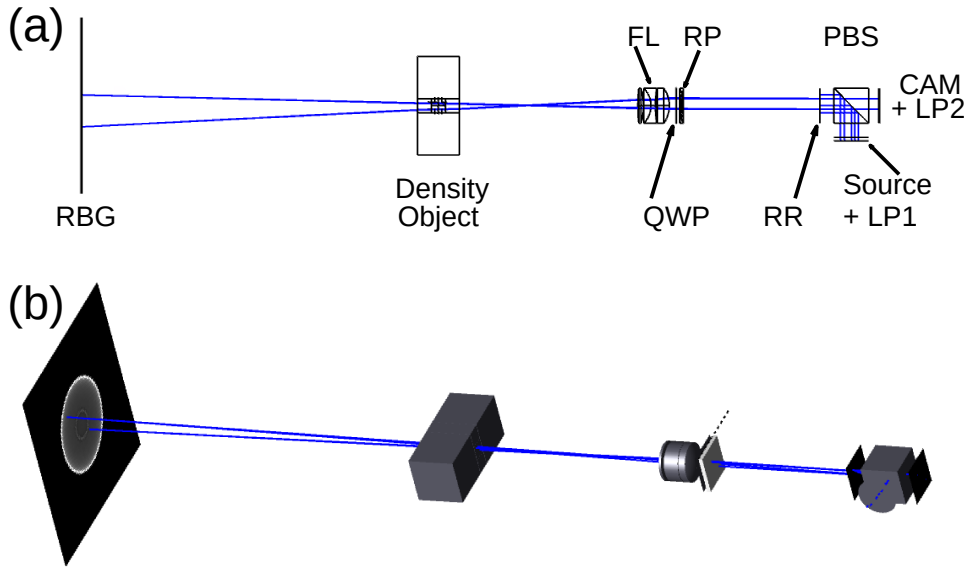

Figure 4. (a) Labelled wireframe SAFS model in Zemax and (b) 3D shaded isometric view of SAFS model in Zemax. Both models use 5 layout rays here for the purpose of ray path visualization.

by a table. In each schematic shown in Fig. 4, the density object is built with 18 cubes, 8 with the simulated refractive index data and 10 with ambient index data, each with $n_x = n_y = n_z = 83$ to satisfy the limitation in Eq. (2) The initial position of each SAFS component was determined using the assistive tool for self-aligning schlieren (ATLAS) (N. Mejia & Schmidt, 2023).

4. Results

Three ANSYS Zemax simulations using refractive index fields from a compressible flow obtained from CFD are presented. The first simulation is of a hypersonic stagnation point injection (SPI) flow configuration (N. A. Mejia & Schmidt, 2022; N. Mejia et al., 2024). A sonic jet of air issues from the center of a hemispherical forebody into a Mach 6 freestream, which goes from left to right in Fig. 5. Only the top half of the hemispherical body is shown in the bottom right of the images and is outlined by the dashed orange line. The refractive index field was computed using the CHAMPS solver (Brehm et al., 2015, 2019) with 5×10^7 analysis rays, which is compared to a numerical path-integrated conventional schlieren image of the field (Fig. 5b). Here, key features of the SPI flow are captured in the Zemax simulation (Fig. 5a) using 4 million analysis rays. The bow shock (asterisk), Mach disk (plus sign), contact surface (diamond), and shear layers (triangle) are visible, and Zemax is able to capture features such as the bulge in the upper area of the bow shock and some turbulent flow features between the bow shock and model. Due to implementation limitations with the grid gradient feature in Zemax, the physical wind tunnel model in this Zemax simulation is ambient air, rather than an absorbing or reflecting surface, which is why it transmits light. In the Zemax image, there are long, curved features (striations) between the model and the

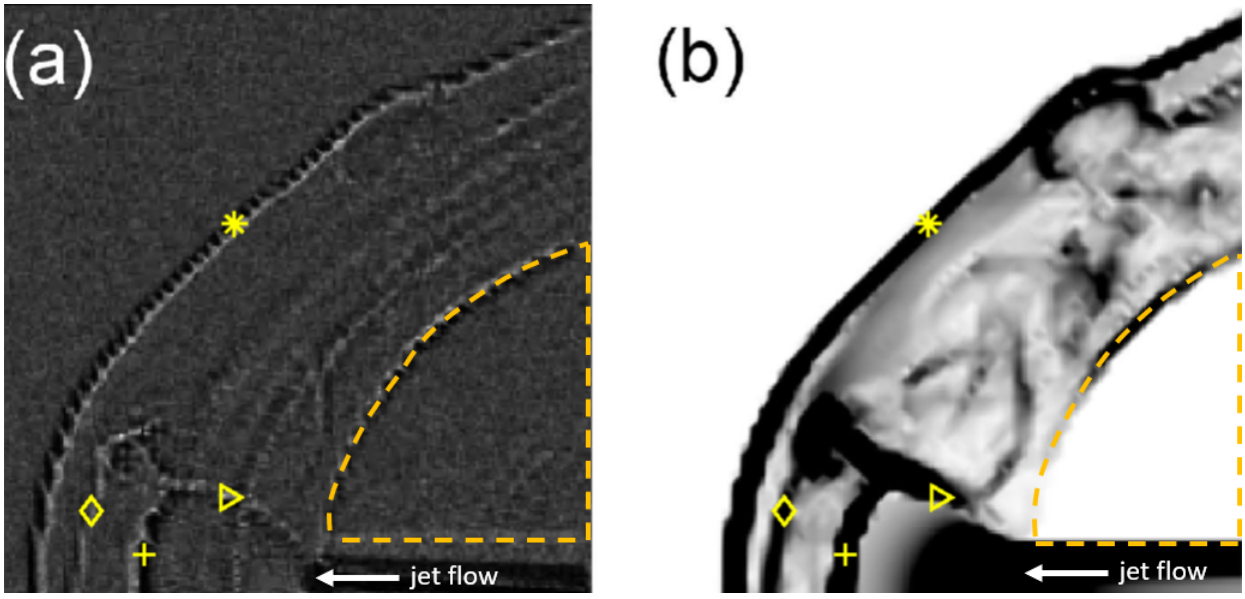

Figure 5. Results of a simulated SPI refractive index field shown as a (a) Zemax SAFS model ray trace and (b) path-integrated numerical schlieren image. Each label denotes a region of interest that is called out in the text and area enclosed in the dashed lines is the model.

bow shock that are not present in the synthetic schlieren image from the CFD or the experimental image. These may be artifacts from the three-dimensional bow shock along the line of sight. The numerical CFD data uses a Cartesian grid that is not shock-aligned, which can result in a stair-stepping pattern that is then accentuated by the sub-sampling used for the GGO.

The second simulation is also of an SPI flow configuration, but the Zemax simulation uses 4×10^9 analysis rays (the maximum allowed by Zemax), and it is compared to experimental conventional, path-integrated schlieren data taken from the experiments conducted by N. Mejia et al. (2024). Both images are shown in Fig. 6. In the Zemax simulation image (Fig. 6a), a ray-absorbing sphere was placed at the model location in Zemax in order to mimic the effect of the physical model terminating rays in the conventional schlieren system. Here, the Zemax simulation captures complex features such as the contact surface, Mach disk, shear layers, bow shock, and a vortex-shed shear layer. The image still exhibits the striations behind the shock due to the aforementioned CFD data using a Cartesian grid which is not shock-aligned, but the image shows great promise in simulating a schlieren image, especially when compared to that of the numerical schlieren image in Fig. 5b.

The third simulation is of a shock wave created by laser-induced breakdown from Ref. Bathel et al. (2021) with 4×10^7 analysis rays. This is compared to an experimental conventional, path-integrated schlieren image shown in Fig. 7. The shock front appears at the top of the Zemax simulation (Fig. 7a) and appears similar to the feature in the conventional schlieren image in Fig. 7b. The Zemax image is slightly blurry because of the relatively low number of rays and large step size (i.e., the magnitude of discretization of the ray tracing equations through the refractive index

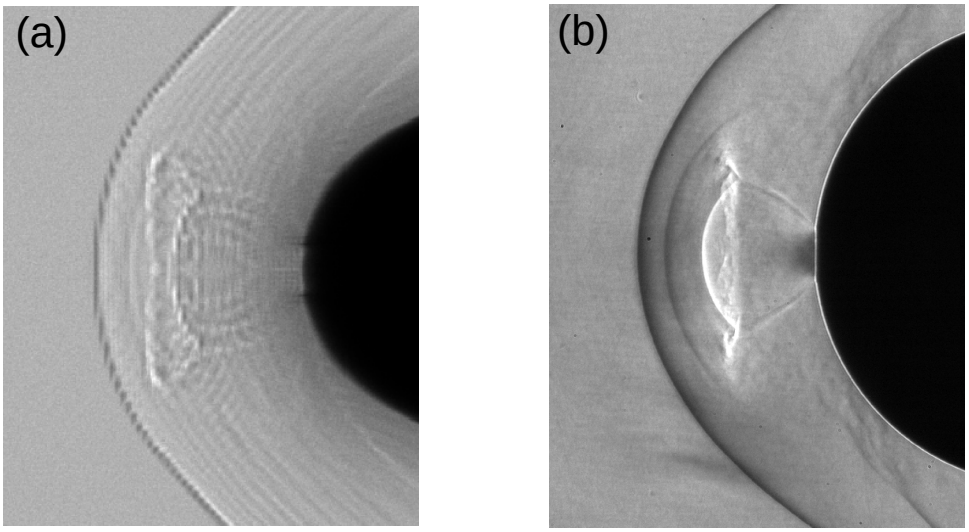

Figure 6. Results of a simulated SPI refractive index field shown as (a) a Zemax model ray trace and (b) an experimental schlieren image.

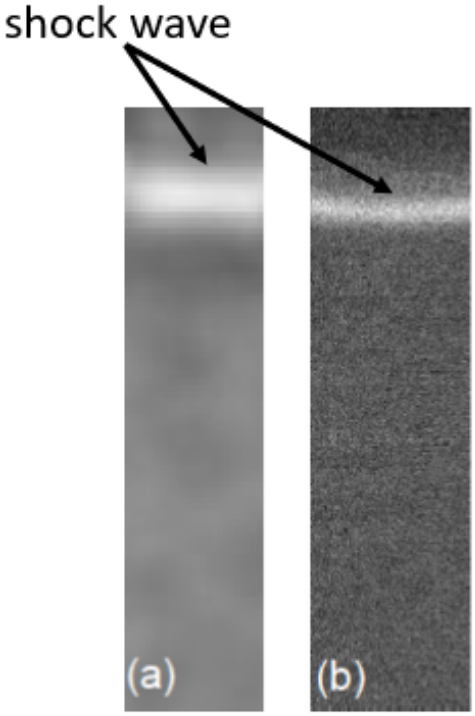

Figure 7. (a) Zemax simulation of shock front. (b) Conventional path-integrated schlieren image of a shock front.

field) used for computation. A defining feature of a self-aligned schlieren system is its ability to image a narrow depth of field and so the Zemax simulation should also exhibit this feature. While measurements were not recorded, the authors do note that the system is sensitive to translation of the density object along the optical axis as one would expect.

5. Conclusion

Modeling of a self-aligned focusing schlieren system has been performed in Zemax with simulated refractive index fields from compressible flows as the subject. Details on implementation of each of the optics have been included with additional discussion for objects that are more complex to implement. The density object was implemented using multiple grid gradient objects as subdomains of the simulated compressible flow field. This technique allows the user to bypass a limit in Zemax for the number of points in the refractive index field. As the number of GGOs increases, the cost of the simulation increases significantly. Additionally, the retroreflective background performance was obtained by modifying a scatter-defining function DLL in Zemax in order to scatter the rays back towards the incident ray rather than the specular ray. The Ronchi ruling was built using a MATLAB script to create a high resolution bitmap image representing the line pairs and imported into Zemax using the slide object.

Zemax simulations of a hypersonic stagnation point injection flow configuration were compared to both a numerical schlieren image and an experimental schlieren image. The Zemax simulations are able to capture fine details in the flow such as the Mach disk, shear layers, contact surface, and bow shock. An artifact of the CFD Cartesian grid not being shock-aligned appears as striations behind the bow shock. A Zemax-simulated focusing schlieren image from a shock wave from laser-induced breakdown is also compared to an experimental image and appears qualitatively similar, but is blurred due to the large step size used for the computational data.

In future work, it would be valuable to see how computational data specifically designed to be visualized in Zemax would perform. In particular, if it would be possible to rid the image of the striation artifacts seen in the SPI images. Additionally, a more efficient and automated method of implementing the density object GGOs is necessary to simulate finer and more complex refractive index fields.

Acknowledgements

The authors acknowledge the financial support from the Air Force Office of Scientific Research under Grant No. FA9550-22-1-0374. Support for Nicholas Mejia while in residence at NASA Langley Research Center performing the preliminary simulation work was provided by NASA's Hypersonic Technology Project (HTP). Support for the Zemax software used for initial simulation work was provided by Lisa Le Vie of NASA Langley Research Center's Advanced Measurements and Data Systems Branch. Additional support for self-aligned focusing schlieren development provided by NASA's Transformational Tools and Technologies (T^3) Project.

References

Ammann, E. O., & Massey, G. A. (1968). Modified forms for glan–thompson and rochon prisms*†. *Journal of the Optical Society of America*, *58*(11), 1427. doi: 10.1364/josa.58.001427

Bathel, B. F., & Weisberger, J. M. (2021, July). Compact, self-aligned focusing schlieren system. *Optics Letters*, *46*(14), 3328. doi: 10.1364/ol.428011

Bathel, B. F., Weisberger, J. M., Herring, G. C., Jagannathan, R., Johansen, C. T., Jones, S. B., & Cavone, A. A. (2021, January). Analysis of the amplitude response of a two-point and a multi-point focused laser differential interferometer. In *AIAA scitech 2021 forum.* doi: 10.2514/6.2021-0598

Boedeker, L. R. (1959). *Analysis and Construction of a Sharp Focussing Schlieren System* (Unpublished master's thesis). Massachusetts Institute of Technology.

Brehm, C., Barad, M. F., & Kiris, C. C. (2019, July). Development of immersed boundary computational aeroacoustic prediction capabilities for open-rotor noise. *Journal of Computational Physics*, *388*, 690-716. doi: 10.1016/j.jcp.2019.02.011

Brehm, C., Hader, C., & Fasel, H. F. (2015, August). A locally stabilized immersed boundary method for the compressible navier–stokes equations. *Journal of Computational Physics*, *295*, 475-504. doi: 10.1016/j.jcp.2015.04.023

Burton, R. A. (1949, nov). A Modified Schlieren Apparatus for Large Areas of Field. *Journal of the Optical Society of America*, *39*(11), 907. doi: 10.1364/josa.39.000907

Gladstone, J., & Dale, T. (1863, dec). XIV. Researches on the refraction, dispersion, and sensitiveness of liquids. *Philosophical Transactions of the Royal Society of London*, *153*, 317–343. doi: 10.1098/rstl.1863.0014

Hartmann, J. (1940, November). *The Acoustic Air-Jet Generator* (Technical Translation (2021) No. NASA-TT-20210016495).

Héricz, D., Sarkadi, T., Erdei, G., Lazuech, T., Lenk, S., & Koppa, P. (2017). Simulation of small-and wide-angle scattering properties of glass-bead retroreflectors. *Applied Optics*, *56*(14), 3969–3976. doi: 10.1364/AO.56.003969

Hill, J. L., Borg, M. P., Benitez, E. K., Running, C. L., & Reeder, M. F. (2023). Implementation of self-aligned focusing schlieren for hypersonic boundary layer measurements. In *Aiaa scitech 2023 forum.* doi: 10.2514/6.2023-2438

Jenkins, F. A., & White, H. E. (1976). *Fundamentals of optics* (4th ed.; R. A. Fry & A. T. Vinnicombe, Eds.). McGraw-Hill Book Company.

Mejia, N., & Schmidt, B. E. (2023, January). Atlas: Assistive tool for self-aligning schlieren. In *AIAA scitech 2023 forum.* doi: 10.2514/6.2023-2265

Mejia, N., Schmidt, B. E., DeFazio, D., Jewell, J. S., Chinske, C. C., McQuaid, J. A., & Brehm, C. (2024, January). *Flow interaction dynamics of stagnation point injection in Mach 6 quiet flow.* American Institute of Aeronautics and Astronautics. doi: 10.2514/6.2024-1751

Mejia, N. A., & Schmidt, B. E. (2022, sep). Experimental investigation of flow interaction dynamics in supersonic retropropulsion. *Journal of Spacecraft and Rockets*, *59*(5), 1753–1762. doi: 10.2514/1.a35228

Schardin, H. (1942). *Schlieren methods and their applications* (NASA-TT-F12731 (1970)).

Settles, G. S. (2001). *Schlieren and shadowgraph techniques* (First ed.). Springer Berlin Heidelberg.

Settles, G. S., & Hargather, M. J. (2017). A review of recent developments in schlieren and shadowgraph techniques. *Measurement Science and Technology*, *28*. doi: 10.1088/1361-6501/aa5748

Wang, Y., & Kulatilaka, W. D. (2017, April). Optical ray tracing method for simulating beam-steering effects during laser diagnostics in turbulent media. *Applied Optics*, *56*(11), E106. doi: 10.1364/ao.56.00e106

Weinstein, L. M. (1993, jul). Large-field high-brightness focusing schlieren system. *AIAA Journal*, *31*(7), 1250–1255. doi: 10.2514/3.11760

Weisberger, J. M., & Bathel, B. F. (2022a). Characterization of rochon prisms for bi-directional imaging applications. *NASA/TM–20210026232*.

Weisberger, J. M., & Bathel, B. F. (2022b). Single source/cutoff grid, self-aligned focusing schlieren system. *Experiments in Fluids*, *63*(8). doi: 10.1007/s00348-022-03389-7